Title

Resonance signatures in the body-frame valence photoionization of CF 4

Journal

Physical Chemistry Chemical Physics, 20(32)

ISSN

0956-5000

Authors

Larsen, KA
Trevisan, CS
Lucchese, RR
et al.

Publication Date

2018-08-15

DOI

10.1039/c8cp03637c

Peer reviewed

Journal Name

ARTICLE TYPE

Cite this: DOI: 10.1039/xxxxxxxxxx

Signatures of quantum interference in the valence photoionization of CF_4

K. A. Larsen,[a,b] C. Trevisan,[c] R. Lucchese,[a] S. Heck,[a,d,e] W. Iskandar,[a] E. Champenois,[a,b] A. Gatton,[a,f] R. Moshammer,[d] R. Strom,[f] T. Severt,[g] B. Jochim,[g] D. Reedy,[h] M. Weller,[e] A. Landers,[f] J. B. Williams,[h] I. Ben-Itzhak,[g] R. Dörner,[e] D. Slaughter,[a] C. W. McCurdy,[a,i] Th. Weber[a,†] and T. N. Rescigno[a,‡]

Received Date
Accepted Date

DOI: 10.1039/xxxxxxxxxx

www.rsc.org/journalname

We present a combined experimental and theoretical investigation of the electron dynamics and body-frame angular dependence of valence photo-single ionization of CF_4 and subsequent dissociation into CF_3^+ and F. Ionization from a valence t_2 orbital shows overlapping shape resonances close to threshold that couple to the same total symmetry, leading to striking quantum interference effects that can be seen in the recoil-frame photoelectron angular distributions.

1 Introduction

Angular distributions of photoelectrons measured in the body-frame of the molecule are rich in detail and can yield far more information than conventionally measured laboratory-frame photoelectron angular distributions, which are typically characterized by a single asymmetry parameter. Recent examples include molecular imaging with photoejected electrons from core-level ionization [1], imaging electron and/or nuclear dynamics via time-resolved photoelectron spectroscopy [2–4], and observation of core-hole localization in molecules with symmetry equivalent atoms [5].

To measure photoelectron angular distributions in the body-frame, the orientation of the target at the instant of photoionization must be established. This can be achieved through 3-D laser alignment when feasible [6] or, in the case of dissociative ionization, reconstructed through coincident electron-ion momentum imaging techniques, such as COLTRIMS (COLd Target Recoil Ion Momentum Spectroscopy) [7]. In the latter case, the time scale for fragmentation must be short compared to the rotational period of the molecule so that the molecular orientation at the instant of photoionization can be deduced from the product ion momenta. This condition is generally referred to as the axial recoil approximation.

Laser alignment prior to photoionization is limited to molecules with an asymmetric polarizability and thus not applicable to a highly symmetric molecule such as CF_4. Moreover, photoelectron-photoion coincidence studies have established that valence photoionization of CF_4 leading to the ground-state and two lowest electronically excited states of CF_4^+ result in CF_3^+ + F products. The COLTRIMS technique is therefore uniquely capable of accessing the dissociative photoionization dynamics of CF_4.

Resonances are seen in the photoionization continuum of many small molecules. Features in narrow resonances are sensitive to the excitation energy and are often sensitive to molecular geometry. Often such resonances can exhibit interesting features in their differential cross sections based on the interference between resonant and non-resonant pathways to the same final state. For example, a rapid change in the sign of circular dichroism for valence-shell ionization of N_2O has been observed as the photon energy is swept across the lowest Rydberg resonance embedded in the continuum [8]. There are also striking examples of left/right symmetry breaking in the dissociative photoionization of molecular hydrogen [9,10]. The observed asymmetry is the result of such quantum interference between resonant and non-resonant pathways. A similar effect has recently been seen in the dissociative electron attachment to H_2, where overlapping negative ion resonances of opposite parity provide interfering pathways to the same dissociative channel [11].

A striking example of quantum interference is found in the present investigation in which we present the results of a joint

[a] Chemical Sciences Division, Lawrence Berkeley National Laboratory, Berkeley, California 94720.
[b] Graduate Group in Applied Science and Technology, University of California, Berkeley, California 94720, USA.
[c] Department of Sciences and Mathematics, California State University, Maritime Academy, Vallejo, California 94590.
[d] Max-Planck-Institut für Kernphysik, Saupfercheckweg 1, 69117 Heidelberg, Germany.
[e] J.W. Goethe Universität, Institut für Kernphysik, Max-von-Laue-Str. 1, 60438 Frankfurt, Germany.
[f] Department of Physics, Auburn University, Alabama 36849, USA.
[g] J.R. Macdonald Laboratory, Kansas State University, Manhattan, Kansas 66506, USA.
[h] Department of Physics, University of Nevada Reno, Reno, Nevada 89557, USA.
[i] Department of Chemistry, University of California, Davis, California 95616, USA.
† Corresponding author, email: TWeber@lbl.gov
‡ Corresponding author, email: TNRescigno@lbl.gov

experimental and theoretical study of valence photo-single ionization of CF_4 followed by dissociation into CF_3^+ and F. The surprising and totally unexpected result we found is that in certain ionization channels there are narrow overlapping resonances of the *same total symmetry* which give rise to rapid changes in the recoil-frame photoelectron angular distributions over a very narrow electron energy range. Such effects were not seen in previous studies on CF_4 [12] nor, to our knowledge, in any other case involving photoionization of a molecule with high symmetry.

The outline of this paper is as follows. We begin with a brief overview of previous work, both theoretical and experimental, on CF_4 photoionization, along with a summary of recent work on the CF_4^+ dissociation pathways. We then turn to a description of our experimental setup, followed by an outline of the theoretical approach used in this study. We follow with a presentation of our experimental and theoretical results, a detailed analysis of the quantum interference effects we have found and conclude with a brief discussion.

2 Background

The outer four valence molecular orbitals of ground-state CF_4 ($...3t_2^6\ 1e^4\ 4t_2^6\ 1t_1^6$) have vertical ionization potentials of 22.12, 18.50, 17.49 and 16.20 eV, respectively [13,14]. Removal of an electron from one of these orbitals produces CF_4^+ in its C^2T_2, B^2E, A^2T_2 or X^2T_1 state, respectively. Conventional photoelectron-photoion coincidence spectroscopy (PEPICO) [15] and threshold PEPICO [16] studies have established that the lowest three CF_4^+ ion states, X^2T_1, A^2T_2 and B^2E, all decay exclusively to CF_3^+ + F, while the C^2T_2 state dissociates into CF_2^+ + F_2 and CF_2^+ + F + F channels. *Ab initio* calculations have shown that there is a shallow minimum on the ground-state CF_4^+ (X^2T_1) surface [17], which has little effect on the dissociation to CF_3^+ + F products. The A^2T_2 surface, on the other hand, which is evidently steeply repulsive in the Frank-Condon region, shows no minimum and therefore dissociates impulsively [14]. The B^2E state dissociation is more complicated. Since it is bound on its adiabatic potential energy surface [18], its dissociation must occur following either internal conversion or radiative decay to a lower dissociative state. Early speculation that it decays by radiating to the lower A^2T_2 state before dissociating would require a long lifetime that is inconsistent with experimental observations and was disproven by photoelectron-photoion coincidence measurements [19]. It is now thought that the B state undergoes an internal conversion to the A state and then dissociates on the A state surface [14].

Compared to the body of literature on CF_4^+ dissociation dynamics, far less work has been done on CF_4 photoionization cross sections and photoelectron angular distributions. Using angle resolved photoelectron spectroscopy and synchrotron radiation, Carlson *et al.* [20] published partial cross sections and asymmetry parameters for valence photoionization of CF_4. Similar measurements were published a year later by Yates *et al.* [21]. Yates *et al.* also reported theoretical results using the multiple-scattering (MS-Xα) method. A more extensive MS-Xα study was subsequently published by Stephens *et al.* [22]; more recently, another theoretical study was reported using the iterative Schwinger method [23]. In all three studies, integrated cross sections and asymmetry parameters were reported. Of particular relevance to the present work are the narrow shape resonances found close to threshold in the MS-Xα calculations. These resonances were not found in the Schwinger calculations [23] and were stated to be unphysical artifacts of the earlier calculations. We suspect that the use of an empirical correlation-polarization potential in the Schwinger calculations led to an unbalanced treatment that pushed the resonances below their parent ions. To our knowledge, there are no previous theoretical studies of body-frame photoionization for CF_4.

3 Experimental

Valence photoionization measurements on CF_4 were performed using a tunable monochromatic linearly polarized beam of extreme ultraviolet (XUV) photons produced at beamline 10.0.1.3 at the Advanced Light Source (ALS) synchrotron located at Lawrence Berkeley National Laboratory. The beamline monochromator was configured to provide photons with energies between 18.3 - 31.0 eV to the experiment with an energy resolution of less than $\pm$50 meV.

A beam of rotationally and vibrationally cold neutral CF_4 molecules ($\sim 80^\circ$ K) was formed by an adiabatic expansion through a 50 μm nozzle. This expansion was collimated by two skimmers to form a jet that propagated perpendicular to the photon beam. These two beams crossed at the interaction region ($\sim 0.15 \times 0.15 \times 1$ mm^3) inside a 3-D momentum imaging spectrometer, resulting in the photoionization of the neutral ground state CF_4 molecules at a rate of less than one ionization event per XUV pulse, ensuring unambiguous coincidence conditions.

Within a range of photon energies explored (18.3 - 21.4 eV), only the F + CF_3^+ fragmentation was observed, which was investigated using COLTRIMS [7], where the photoelectron and the CF_3^+ ion produced by a photoionization event were collected with full 4π solid angle detection efficiency and their 3-D momenta measured in coincidence. The electrons and ions were guided using parallel static electric (2.4 - 7.0 V/cm) and magnetic (2.2 - 7.9 G) fields to multi-hit capable position- and time-sensitive detectors. Both detectors comprised a multichannel plate (MCP) chevron stack and a delay-line anode readout, each at opposite ends of the spectrometer. The electron and ion delay-line detectors were a three-layer hex-anode [24] with an 80 mm MCP stack and a two-layer quad-anode with a 120 mm MCP stack, respectively. This system encodes both the charge carrier's 3-D momentum into their hit position on the detector and time-of-flight (TOF) relative to the ALS bunch marker.

The data were recorded in list mode on an event-by-event basis, enabling extraction, sorting and transforming the coordinates of each event (TOF and hit position) by a detailed offline analysis. For each dissociative ionization event, the photoelectron kinetic energy and emission angle relative to the recoil axis of the heavy fragments were derived using the measured 3-D electron and recoil-ion momenta. The orientation of the recoil axis at the moment of photoionization and the kinetic energy release (KER) of the fragmentation were calculated assuming conservation of momentum between the measured CF_3^+ ion and the neutral F atom. For average electric and magnetic collection fields of the

spectrometer (∼4.5 V/cm and ∼4 G) the energy resolution for a typical 3 eV photoelectron and 0.25 eV CF_3^+ ion was ≤0.26 eV and ≤0.06 eV, respectively.

The 3-D momentum information is used to generate recoil frame photoelectron angular distributions (RFPADs), which visualize the photoelectron emission patterns in the body-fixed frame of the molecule for a given orientation relative to the polarization of the XUV light. Some ambiguity in the absolute molecular orientation remains, as the orientation of the CF_3^+ ion about the recoil axis is unknown. The generated RFPADs possess an angular resolution of around ∼ 3°.

4 Theoretical

The calculation of molecular frame photoelectron angular distributions (MFPADs) requires a description of both the initial neutral electronic state of the molecule and the electron-ion scattering wave function corresponding to the cationic state of the molecule that is produced. To produce the required continuum wave functions, we used the well-established complex Kohn variational method for electron-molecule scattering[25], with modifications needed to treat electron scattering from molecular ions[26], including coupling between electronic states of the ion. Since the application of the complex Kohn method to photoionization has been described in some detail previously[4,25,27,28], only its salient features are repeated here.

In the present application, the ion states were described by placing a single valance orbital vacancy in the ground-state Hartree Fock wave function of neutral CF_4. If that vacancy is created in an occupied target orbital that has a number of degenerate components, then the electron-ion wave function is expanded as:

$$\Psi^-_{\Gamma_o l_o m_o} = \sum_\Gamma \hat{A}(\chi_\Gamma F^-_{\Gamma\Gamma_o l_o m_o}), \tag{1}$$

where $\hat{A}$ is the antisymmetrization operator, the sum runs over the energetically degenerate components of the ion state in question, denoted by χ_Γ, and $F^-_{\Gamma\Gamma_o l_o m_o}$ is the corresponding photoelectron continuum function, with angular momentum quantum numbers l_o, m_o, for producing ion component Γ_o. Thus coupling between all the components of a degenerate ion state is explicitly included in the close-coupling expansion.

In the complex Kohn method, the continuum functions are further expanded as:

$$\begin{aligned} F^-_{\Gamma\Gamma_o l_o m_o} &= \sum_i c_i^{\Gamma\Gamma_o}\phi_i(r) + \sum_{lm}[f_l(k_\Gamma r)\delta_{ll_o}\delta_{mm_o}\delta_{\Gamma\Gamma_o} \\ &\quad + T^{\Gamma\Gamma_o}_{ll_o mm_o} h^-_l(k_\Gamma r)]Y_{lm}(\hat{r})/r\,, \end{aligned} \tag{2}$$

where f_l and h^-_l are partial-wave continuum radial functions behaving asymptotically as regular and incoming Coulomb functions[26] and ϕ_i is a set of square integrable (Cartesian Gaussian) functions. To construct an amplitude that represents an ionization process for a specific value of ejected electron momentum measured in the molecular body-frame, we combine the functions $\Psi^-_{\Gamma_o l_o m_o}$ in a partial wave expansion:

$$\Psi^-_{\Gamma_0,\vec{k}_{\Gamma_0}} = \sum_{l_0 m_0} i^{l_0}\exp\left[-i\delta_{l_0}(k_{\Gamma_0})\right] Y^*_{l_0 m_0}(\hat{\mathbf{k}})\psi^-_{k,\Gamma_0 l_0 m_0}(\mathbf{r}_1,\cdots,\mathbf{r}_N)\,, \tag{3}$$

where δ_{l_0} is a Coulomb phase shift.

The MFPAD for a fixed direction of the polarization vector $\hat{\varepsilon}$ is related to the dipole matrix element between the neutral and electron-ion scattering wave functions via the relation

$$\frac{d^2\sigma^{\Gamma_0}}{d\Omega_{\hat{k}} d\Omega_{\hat{\varepsilon}}} = \frac{8\pi\omega}{3c}\left|\hat{\varepsilon}\cdot\langle\Psi_0|\hat{\mu}|\Psi^-_{\Gamma_0,\vec{k}_{\Gamma_0}}\rangle\right|^2, \tag{4}$$

which defines the body-frame cross section for polarization $\hat{\varepsilon}$ and ejected electron momentum $\vec{k}_{\Gamma_0}$, leaving the ion in state Γ_0.

It is generally not possible to establish the absolute orientation of a polyatomic molecule in a COLTRIMS experiment when only a single ion fragment is produced. In the present case, under the assumption of an impulsive dissociation following photoionization, only the CF_3^+– F recoil axis can be determined, but not the absolute orientation of CF_3^+ about that axis, as mentioned above. Therefore, to compare with experiment, we calculate a recoil frame photoelectron angular distribution (RFPAD) by numerically averaging the calculated MFPADs about the recoil axis.

5 Results

Figure 1 shows a plot of the measured CF_3^+ yield as a function of photoelectron energy and the F + CF_3^+ kinetic energy release measured at a photon energy of 19.4 eV. The plot clearly shows

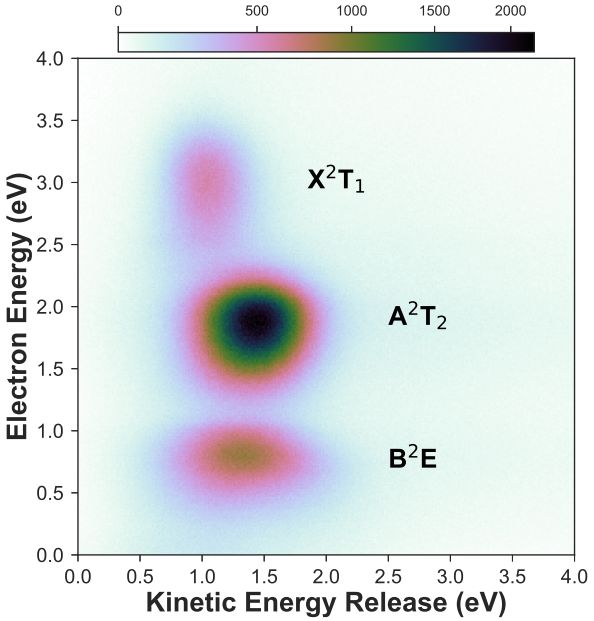

Fig. 1 Measured CF_3^+ yield as a function of photoelectron energy and kinetic energy release in F + CF_3^+ fragmentation for photoionization producing the X^2T_2, A^2T_2 and B^2E states. The photon energy is 19.4 eV.

three distinct islands corresponding to the X^2T_1, A^2T_2 and B^2E CF_4^+ ion channels. It is worth noting that, while the photoelectron energies at the island centers are separated by the vertical

Table 1 Photon energies along with experimental and calculated photoelectron energies (E_{PE}). (See text for an explanation of how these were derived.) All energies in electron volts.

State	$\hbar\omega$	E_{PE} (measured)	E_{PE} (calculated)
$X\,^2T_1$	18.6	2.40 +/- 0.05	2.6
	31.0	14.3 +/- 0.05	15.0
$A\,^2T_2$	18.3	0.94 +/- 0.05	2.1
	18.6	1.15 +/- 0.05	2.4
	19.0	1.53 +/- 0.05	2.8
	19.4	1.89 +/- 0.05	3.2
	20.5	3.16 +/- 0.05	4.3
	21.4	4.20 +/- 0.05	5.2
$B\,^2E$	20.5	2.00 +/- 0.05	3.0
	31.0	12.00 +/- 0.05	13.5

ionization potentials leading to the X, A and B ion states, the corresponding KERs are not. This indicates that there is proportionally more internal energy carried by CF_3^+ in the A and B fragmentation channels than there is in the X channel. Moreover, we see that while the KERs for the X and A states follow their increasing vertical IPs, the peak KER for the B state is evidently smaller than that of the A state. We found this to be true for all the measured photon energies between 18.6 and 22.05 eV (not shown here), which indicates a different dissociation mechanism for the B state. Simple symmetry considerations involving the asymptotic fragments support this conclusion. First consider the observed fragmentation channel. The photon energies employed here only allow for CF_3^+ and F to be formed in their ground electronic states. CF_3^+ is a closed-shell singlet and the F 2p shell is triply degenerate. Therefore, there can only be three asymptotic dissociative CF_4^+ states leading to the ground state of the fragments. In T_d geometry, the X, A, and B CF_4^+ states have degeneracies of three, three, and two, respectively. When one C–F bond is stretched, the symmetry is lowered from T_d to C_{3v}. The $X\,^2T_1$ state splits into E and A_2 components, the $A\,^2T_2$ state splits into A_1 and E components and the $B\,^2E$ state retains E symmetry[18]. The E components of T_1 are lowered, as is the A_1 component of T_2, thus accounting for the three asymptotic states. The B state does not dissociate adiabatically and correlates with excited product states. The B state can therefore only dissociate by radiating to one of the lower states or by undergoing some type of "internal conversion" to the A state. Radiative decay to the A state implies a nanosecond lifetime for the B state, which is inconsistent with the highly asymmetric RFPADs measured for this channel. In any case, it would not be surprising if a partial breakdown of the axial recoil approximation occurs for the formation of CF_3^+ + F in this channel.

We report the partial photoionization cross sections for production of the $(1t_1)^{-1}$, $(4t_2)^{-1}$, and $(1e)^{-1}$ CF_4^+ states as a function of calculated photoelectron energy, noting that some care is needed in relating the theoretical photoelectron energy to the experimental photon energy. The discrepancy between the measured and calculated photoelectron energies is discussed as follows: with dissociatative ion states, the Franck-Condon approximation would lead one to expect, for each ion state, an envelope of allowed photoelectron energies for each photon energy, with the peak cross section corresponding to the vertical ionization energy at the equilibrium geometry of the neutral target:

$$\hbar\omega = E_{\rm ion}^{\rm eq} - E_{\rm target}^{\rm eq} + E_{\rm PE}\,. \tag{5}$$

Thus, the peak signal at a given photon energy and corresponding photoelectron energy, under this assumption, should rise linearly with increasing photon energy. This assumption can break down when resonances are involved, since the photoionization amplitude can then vary rapidly over the Franck-Condon region. The breakdown of the Franck-Condon approximation can be severe when narrow resonances near threshold are involved.

Table 1 lists the photon energies at which measurements were made, the corresponding photoelectron energies at which the peak signals were observed and the theoretical photoelectron energies at which the cross sections were calculated for the best comparison to the experimental data. The latter were chosen by comparing the RFPADs with the experiment at a photon energy away from any resonances and picking the photoelectron energy that gives the best match between the calculated RFPAD and the measured RFPAD at the signal maximum. This is done at the highest photon energy for each state where measurements were made. With this prescription, we find that that the calculated photoelectron energies are approximately 1 eV higher than the experimental energies.

5.1 $1t_1$ ionization

The calculated $1t_1$ total cross section in Fig. 2 shows a prominent $1t_1 \rightarrow kt_2$ resonance at 2 eV photoelectron energy and a broad nonresonant peak centered near 14 eV that is associated primarily with kt_1 and ke continuum states. Similar behavior was found in the MS-Xα calculations of Stephens *et al.*[22]. The resonance positions reported by Stephens *et al.*, in this and other valence channels, are approximately 1 eV lower than the values we find. The measured RFPADs for photon polarization parallel to the recoil axis at 2.6 and 15 eV photoelectron energies are compared

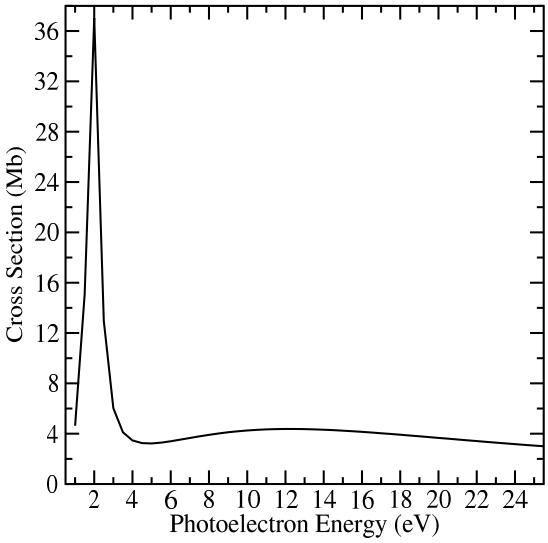

Fig. 2 Computed total cross section for photoionization from the $1t_1$ orbital. 1 Mb = 10^{-18}cm^2

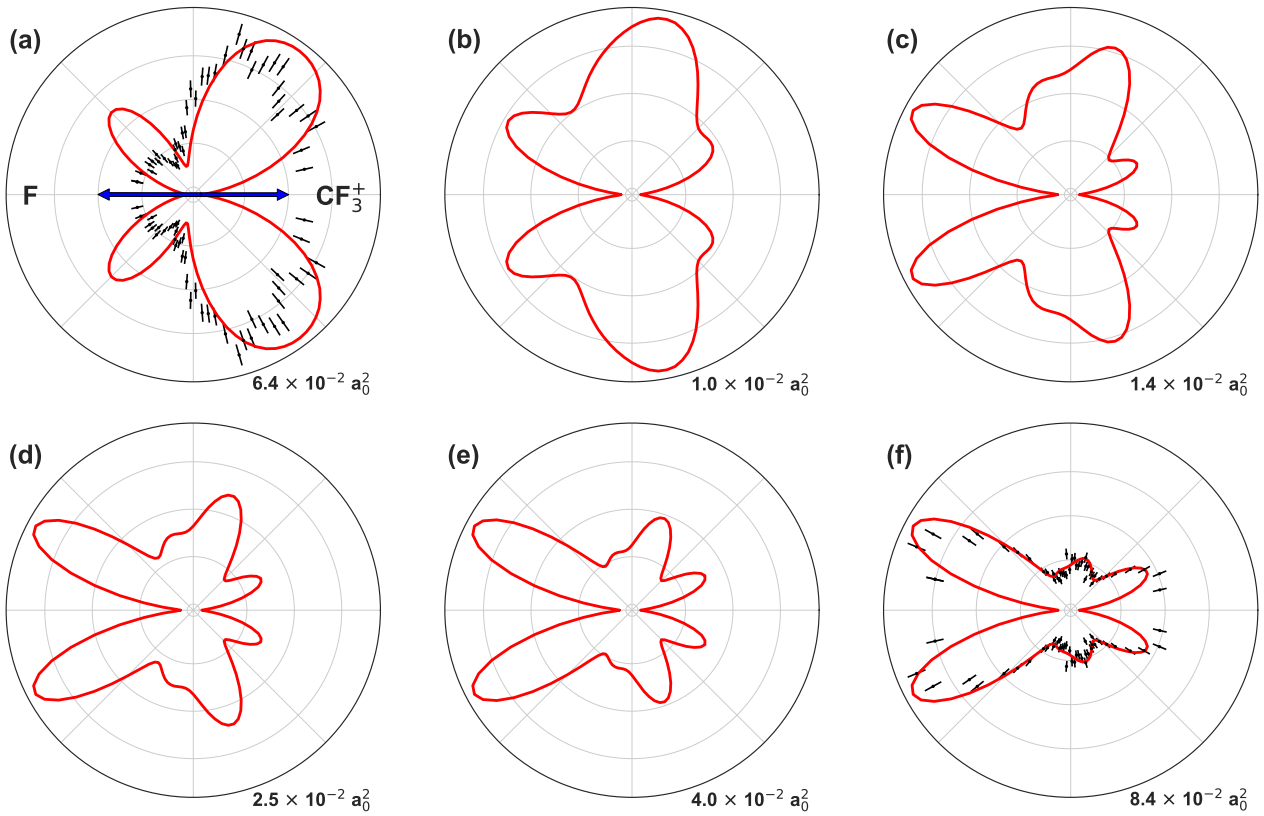

Fig. 3 Experimental (black) and theoretical (red) RFPADs for photoionization from the $1t_1$ orbital of CF_4 at photoelectron energies of (a) 2.6eV and (f) 15.0eV (see Table 1 and text). Calculated RFPADs at photoelectron energies of 4.0, 6.0, 8.0 and 10.0 eV are shown in (b) - (e), respectively. The photon polarization is indicated by the blue arrow. The recoil axis is parallel to the polarization (8° acceptance angle), with the CF_3^+ moving towards 0° and the F moving towards 180°.

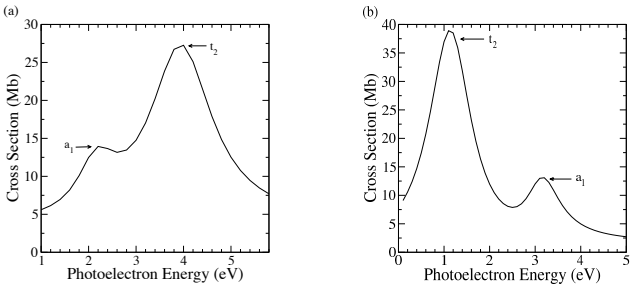

Fig. 4 As in Fig. 2, for photoionization from the (a) $4t_2$ and (b) $3t_2$ orbitals. Resonance peaks are labeled by the symmetry of continuum orbitals involved.

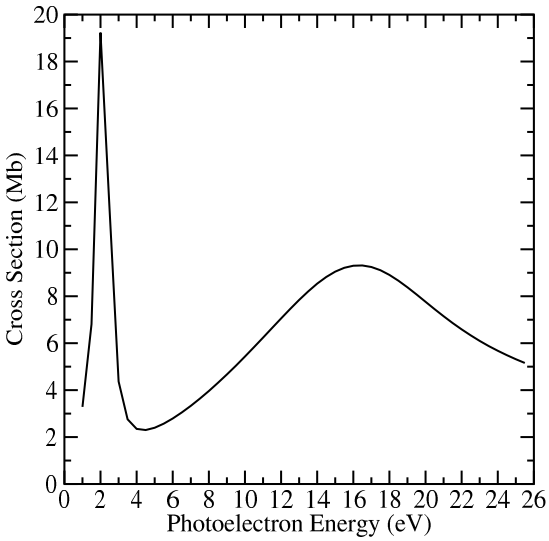

Fig. 6 As in Fig. 2, for photoionization from the 1e orbital.

with theory in Fig. 3. Theoretical results for photoelectron energies between these two extremes are also plotted in Fig. 3 and show a gradual change in shape as we pass from the resonance to nonresonant regions.

5.2 $4t_2$ ionization

The calculated total cross section for the $4t_2$ channel, plotted in Fig. 4a, shows overlapping $4t_2 \rightarrow ka_1$ and $4t_2 \rightarrow kt_2$ resonances centered near 2 and 4 eV, respectively. A comparison of the measured and calculateded RFPADs for this channel is shown in Fig. 5. The striking observation, seen both in theory and experiment, is the apparent flip in the shape of the RFPAD over a narrow energy range. This is in marked contrast to the $1t_1$ channel where the change is gradual.

5.3 1e ionization

Like the $1t_1$ channel, the computed total cross section for the 1e channel, plotted in Fig 6, shows a single $1e \rightarrow kt_2$ resonance at 2 eV photoelectron energy. The RFPADs for this channel are shown in Fig. 7. Once again, we find only a gradual change in the shape of the RFPAD as the photoelectron energy passes from resonance to nonresonant regions. Comparison with experiment is decidedly worse for this channel - a fact we attribute to a partial breakdown of the axial recoil approximation for the reasons given above.

6 Quantum Interference

While shape resonances are common features in the valence photoionization cross sections of many molecules, the case study of CF_4 presented here is not typical. CF_4 is a molecule of high symmetry with degenerate occupied valence orbitals, unstable parent ion states, and massive enough to support narrow shape resonances close to threshold. With its closed-shell $^1A_1$ structure, optical selection rules dictate that only final states (ion + photoelectron) of $^1T_2$ symmetry can be excited. However, with degenerate occupied orbitals, continuum states of different symmetry can be combined with single vacancy target orbitals to produce a state of overall $^1T_2$ symmetry. So, for example, ionization of an occupied t_2 orbital can excite orbital resonance states of a_1 and t_2 symmetry. Since these resonance orbitals can combine with the hole state to produce a neutral (electron + ion) state of $^1T_2$ symmetry, the resonances can interact. The interaction would not be expected to be significant unless the resonances overlap, i.e., their widths sum to an energy greater than their separation. Such appears to be the case with an ionization from the $4t_2$ orbital.

To gain further insight into the nature of these interfering resonances, we carried out two series of single-channel calculations, which only contained continuum contributions from a_1 and t_2 symmetry, respectively. These calculations were carried out using the Schwinger variational method in the static-exchange approximation using the ePolyscat set of codes[29,30]. The RFPADs for the separated $4t_2 \rightarrow ka_1$ and $4t_1 \rightarrow kt_2$ channels obtained from the calculations, each at its corresponding resonance peak maximum, are shown in Fig. 8. These RFPADs bear some qualitative resemblance to the behavior seen in the fully coupled calculations as the photoelectron energy passes from the lower a_1 resonance to the higher t_2 resonance. This illustrates why the true RFPADs undergo a flip in shape. However, we must emphasize that quantitative agreement with the experiment can only be achieved in a fully coupled calculation with all three degenerate components of the $4t_2$ orbital included as ion hole states. The importance of the inclusion of the coupling between nearly degenerate shape resonances of the same total symmetry for the accurate description of RFPADs found here is similar to the strong inter-channel coupling effects seen in the total photoionization cross sections in the resonant near-threshold valence ionization of the linear alkynes.[31]

It is interesting to compare the case of $4t_2$ ionization with that of $3t_2$ ionization. The computed total cross sections for the latter are shown in Fig. 4b. Note that the total cross section for $3t_2$ again shows, as for $4t_2$, two resonances separated by 2 eV. But they are lower in energy by 1 eV, somewhat narrower and their order is reversed from the $4t_2$ case with the t_2 resonance

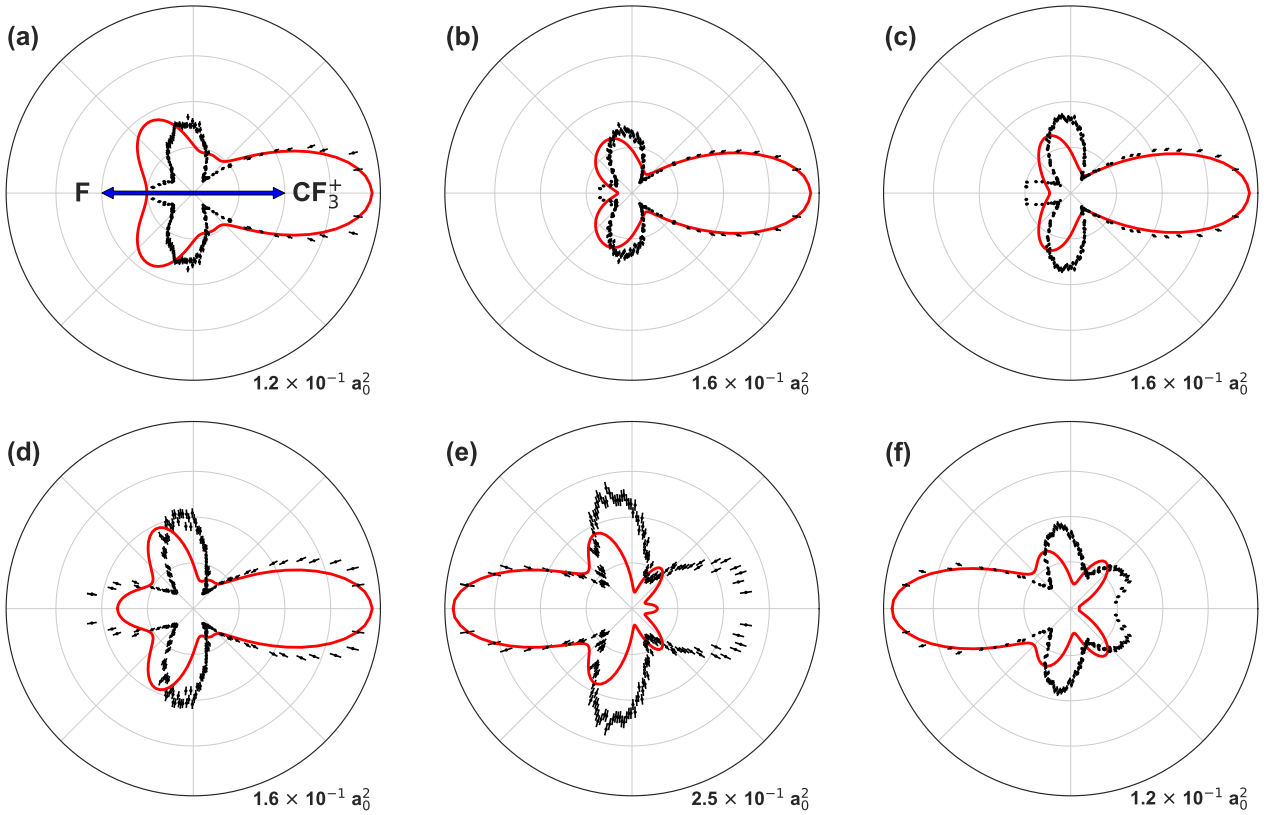

Fig. 5 Experimental (black) and theoretical (red) RFPADs for photoionization from the $4t_2$ orbital of CF_4. The theoretical data in (a) - (f) corresponds with photoelectron energies 2.1eV, 2.4eV, 2.8eV, 3.2eV, 4.3eV and 5.2eV, respectively (see Table 1 and text). The photon polarization is indicated by the blue arrow. The recoil axis is parallel to the polarization (15° acceptance angle), with the CF_3^+ moving towards 0° and the F moving towards 180°.

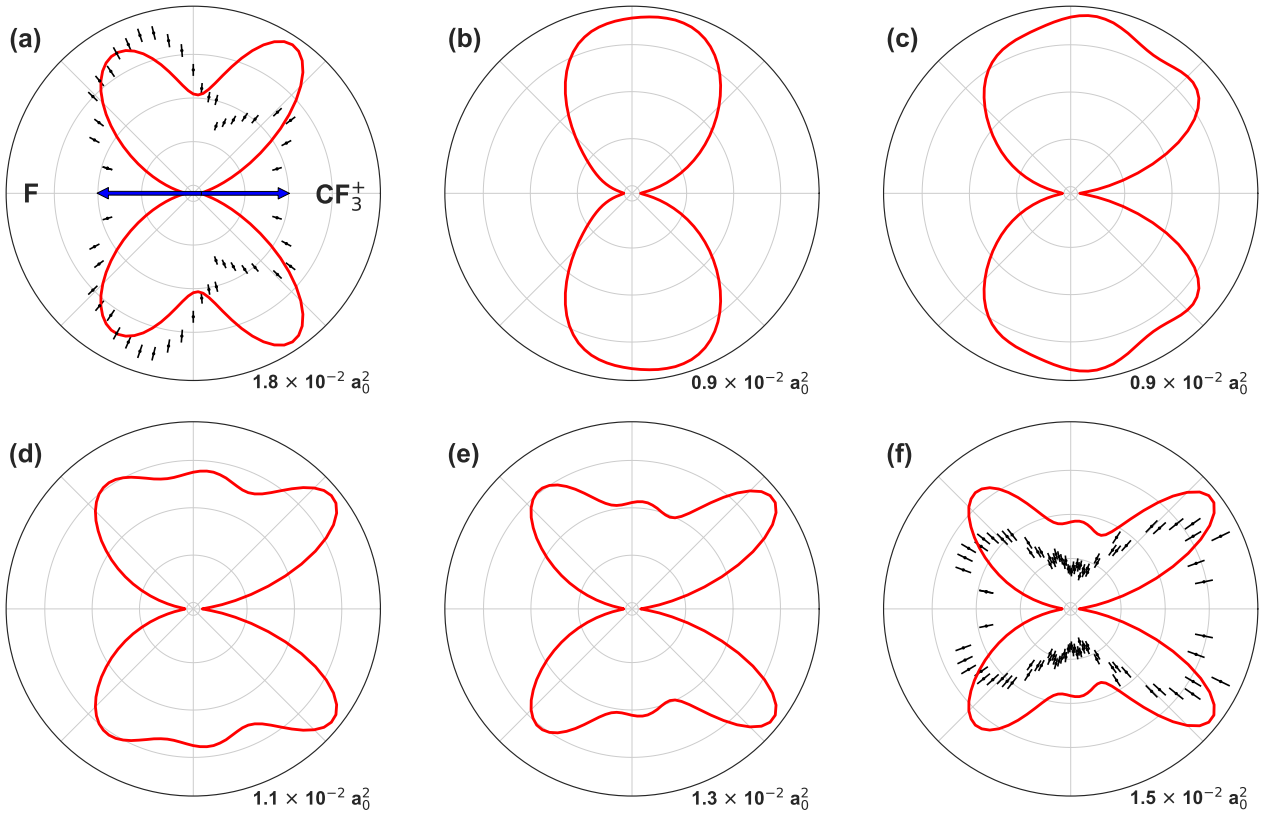

Fig. 7 As in Fig. 3, for 1e ionization at photoelectron energies of (a) 3.0 eV and (f) 13.5 eV. Calculated RFPADs at photoelectron energies of 5.0, 7.0, 9.0 and 11.0 eV are shown in (b) - (e), respectively.

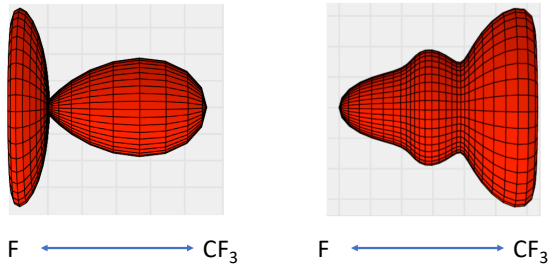

Fig. 8 Computed RFPADs for $4t_2$ ionization from single-channel calculations with continuum contributions of a_1 (left) or t_2 symmetry (right). Both contributions shown at the respective peak energies.

now closer to threshold. The calculated RFPADs for this case are shown in Fig. 9. Not surprisingly, the RFPAD undergoes a change in shape as the energy moves from the lower t_2 resonance to the upper a_1 resonance, but there is no sudden flip in shape as seen in the $4t_2$ case. We also carried out single-channel calculations for the case with continuum contributions from a_1 and t_2 symmetry included separately. The RFPADs for the separated $3t_2 \rightarrow ka_1$ and $4t_1 \rightarrow kt_2$ channels are shown in Fig. 10. The major difference we find is in the t_2 component of the RFPAD, which shows little of the forward/backward asymmetry that causes the apparent flip in the case of $4t_2$ ionization. We should also mention that taking an incoherent sum of the single-channel results for the $3t_2$ ionization produces an RFPAD fairly close to the fully coupled result. This is undoubtedly due to the fact that the a_1 and t_2 resonances are narrower in this case and thus their overlap is reduced. Thus the observation of quantum interference is small. By way of contrast, we found that the sudden flip that occurs in the $4t_2$ ionization channel is strong enough to be seen in the RFPADs even when integrated over all polarization directions relative to the observed fragmentation axis. This is demonstrated in Fig. 11.

7 Conclusions

Body-frame photoelectron angular distributions from valence photoionization of the highly symmetric molecule CF_4 show shape resonances close to threshold. This finding confirms the earlier predictions of Stephens *et al.* [22], contradicting those of the

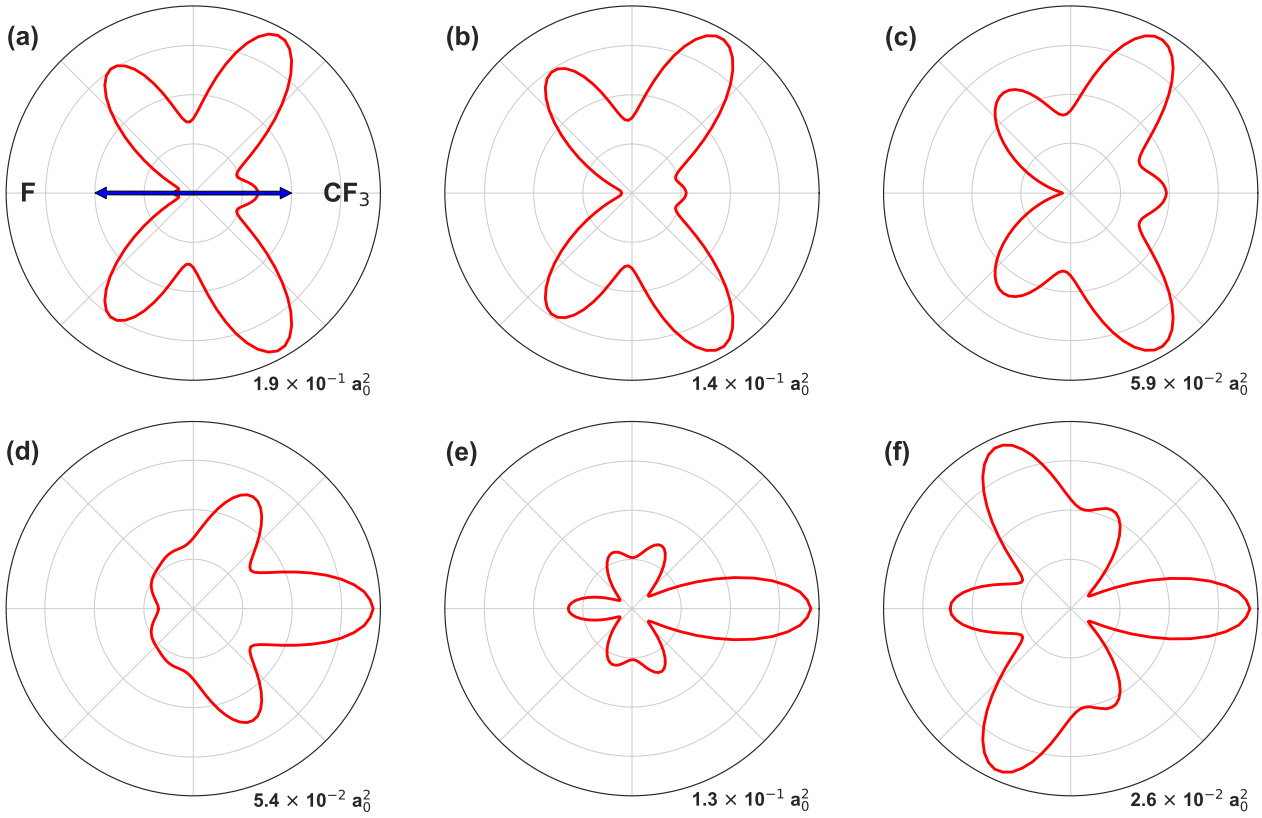

Fig. 9 As in Fig. 3, for $3t_2$ ionization. Calculated RFPADs at photoelectron energies of 1.0, 1.5, 2.0, 2.5, 3.0 and 4.0 eV are shown in panels (a) - (f), respectively. Note that the $3t_2$ ionization channel is not observed to dissociate to CF_3^+ + F. The arrow in panel (a) merley indicates the body-frame orientation used in the fixed-nuclei calculations.

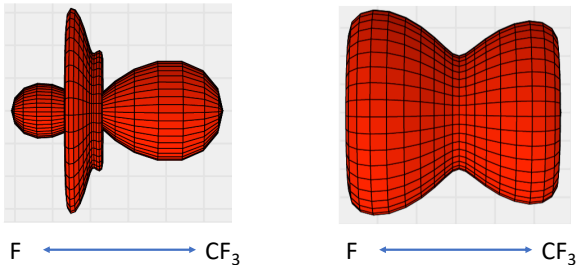

Fig. 10 Computed RFPADs for $3t_2$ ionization from single-channel calculations with continuum contributions of a_1 (left) or t_2 symmetry (right). Both contributions shown at the respective peak energies.

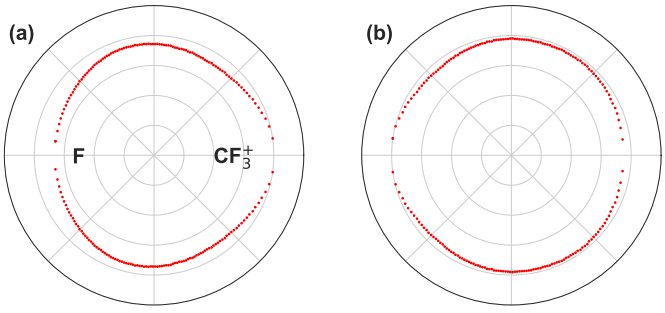

Fig. 11 Measured RFPADs for $4t_2$ ionization at (a) 19.0 and (b) 21.4 eV photon energy, integrated over all polarization directions relative to the observed fragmentation axis.

more recent Schwinger calculations[23] which claimed the resonances to probably be unphysical. The body-frame measurements presented here, and their close agreement with *ab initio* calculations, show these resonances to be real. When ionization takes place from a valence t_2 orbital, there are resonances of both a_1 and t_2 symmetry that couple to the same total symmetry and can thus interfere if sufficiently close in energy. We found this to be the case with the $4t_2$ ionization, where the measured RFPAD undergoes an apparent flip in shape over a narrow photoelectron energy range. This observation represents a striking example of quantum interference not previously observed in molecular valence photoionization.

Conflicts of interest

There are no conflicts to declare.

Acknowledgements

Work at LBNL was performed under the auspices of the US Department of Energy (DOE) under Contract DE-AC02-05CH11231, using the Advanced Light Source and National Energy Research Computing Center, and was supported by the U.S. DOE Office of Basic Energy Sciences, Division of Chemical Sciences. JRML personnel were supported by the same US DOE funding source under Award No. DE-FG02-86ER13491. CST was supported in part by a Berkeley Lab Undergraduate Faculty Fellowship (BLUFF). A.G. was supported by the ALS through a Doctoral Fellowship in Residence. The Frankfurt group acknowledges the support of the Deutsche Akademische Austausch Dienst (DAAD) and the Deutsche Forschungsgemeinschaft (DFG).

Notes and references

1 J. B. Williams, C. S. Trevisan, M. S. Schöffler, T. Jahnke, I. Bocharova, H. Kim, B. Ulrich, R. Wallauer, F. Sturm, T. N. Rescigno, A. Belkacem, R. Dörner, T. Weber, C. W. McCurdy and A. L. Landers, *Phys. Rev. Lett.*, 2012, **108**, 233002.

2 Y. Arasaki, K. Takatsuka, K. Wand and V. McKoy, *J. Chem. Phys*, 2010, **132**, 124307.

3 P. Hockett, C. Z. Bisgaard, O. J. Clarkin and A. Stolow, *Nature Phys.*, 2011, **7**, 612.

4 T. N. Rescigno, N. Douguet and A. E. Orel, *J. Phys. B*, 2012, **45**, 194001.

5 C. W. McCurdy, T. N. Rescigno, C. S. Trevisan, R. R. Lucchese, B. Gaire, A. Menssen, M. S. Schöffler, A. Gatton, J. Neff, P. M. Stammer, J. Rist, S. Eckart, B. Berry, T. Severt, J. Sartor, A. Moradmand, T. Jahnke, A. L. Landers, J. B. Williams, I. Ben-Itzhak, R. Dörner, A. Belkacem and T. Weber, *Phys. Rev. A*, 2017, **95**, 011401.

6 J. L. Hansen, L. Holmegaard, L. Kalhøj, S. L. Kragh, H. Stapelfeldt, F. Filsinger, G. Meijer, J. Küpper, D. Dimitrovski, M. Abu-samha, C. P. J. Martiny and L. B. Madsen, *Phys. Rev. A*, 2011, **83**, 023406.

7 J. Ullrich, R. Moshammer, A. Dorn, R. Dörner, L. P. H. Schmidt and H. Schmidt-Böcking, *Rep. Prog. Phys.*, 2003, **66**, 1463.

8 M. Lebech, J. C. Houver, D. Dowek and R. R.Lucchese, *Phys. Rev. Lett.*, 2006, **96**, 073001.

9 A. Lafosse, M. Lebech, J. C. Brenot, P. M. Guyon, L. Spielberger, O. Jagutzki, J. C. Houver and D. Dowek, *J. Phys. B*, 2003, **36**, 4683.

10 F. Martín, J. Fernández, T. Havermeier, L. Foucar, T. Weber, K. Kreidi, M. Schöffler, L. Schmidt, T. Jahnke, O. Jagutzki, A. Czasch, E. P. Benis, T. Osipov, A. L. Landers, A. Belkacem, M. H. Prior, H. Schmidt-Böcking, C. L. Cocke and R. Dörner, *Science*, 2007, **315**, 629.

11 E. Krishnakumar, V. S. Prabhudesai and N. J. Mason, *Nature Phys.*, 2018, **14**, 149.

12 T. Kinugawa, Y. Hikosaka, A. M. Hodgekins and J. H. D. Eland, *J. Mass Spectrom.*, 2002, **37**, 854.

13 A. J. Yencha et al., *J. Mass Spec. Rel. Phen.*, 1994, **70**, 29.

14 X. Tang, X. Zhou, M. Wu, Z. Gao, S. Liu, F. Liu, X. Shan and L. Sheng, *J. Chem. Phys.*, 2013, **138**, 094306.

15 I. G. Simm, C. J. Danby, J. H. D. Eland and P. I. Mansell, *J. Mass Spec. Rel. Phen.*, 1976, **72**, 29.

16 J. C. Creaset, H. M. Joses, D. M. Smith, R. P. Tuckett, P. A. Hatherly and K. Codling, *Chem. Phys.*, 1993, **174**, 441.

17 H. Tachikawa, *J. Phys. B*, 2000, **33**, 2367.

18 R. A. Beärda and J. J. C. Mulder, *Chem. Phys.*, 1988, **128**, 479.

19 J. P. Maier and F. Thommen, *Chem. Phys. Letts.*, 1980, **78**, 54.

20 T. Carlson, A. Fahlman, W. A. Svensson, M. O. Krause, T. A. Whitley, F. A. Grimm, M. N. Piancastelli and J. W. Taylor, *J. Chem. Phys.*, 1984, **81**, 3828.

21 B. W. Yates, K. H. Tan, G. M. Bancroft, L. L. Coatsworth and J. S. Tse, *J. Chem. Phys.*, 1985, **83**, 4906.

22 J. A. Stephens, D. Dill and J. L. Dehmer, *J. Chem. Phys.*, 1986, **84**, 3638.

23 E. M. Nascimento, L. E. Machado, L. M. Brescansin and Lee, M. -T., *J. Elec. Spec. Rel. Phen.*, 2003, **130**, 101.

24 O. Jagutzki, A. Cerezo, A. Czasch, R. Dörner, M. Hattaß, M. Huang, V. Mergel, U. Spillmann, K. Ullmann-Pfleger, T. Weber, H. Schmidt-Böcking and G. D. W. Smith, *IEEE Trans. Nucl. Sci.*, 2002, **49**, 2477.

25 T. N. Rescigno, B. H. Lengsfield and A. E. Orel, *J. Chem. Phys.*, 1993, **99**, 5097.

26 A. Orel, T. N. Rescigno and B. H. Lengsfield III, *Phys. Rev. A*, 1990, **2**, 5292.

27 S. Miyabe, C. W. McCurdy, A. E. Orel and T. N. Rescigno, *Phys. Rev. A*, 2009, **79**, 053401.

28 C. S. Trevisan, C. W. McCurdy and T. N. Rescigno, *J. Phys. B*, 2012, **45**, 194002.

29 F. A. Gianturco, R. R. Lucchese and N. Sanna, *J. Chem. Phys.*, 1994, **100**, 6464–6471.

30 A. P. P. Natalense and R. R. Lucchese, *J. Chem. Phys.*, 1999, **111**, 5344–5348.

31 U. Jacovella, D. M. Holland, S. Boye-Peronne, B. Gans, N. de Oliveira, K. Ito, D. Joyeux, L. E. Archer, R. R. Lucchese, H. Xu and S. T. Pratt, *J. Phys. Chem. A*, 2015, **119**, 12339–48.